Applied Catalysis B: Environmental 251 (2019) 112–118

Contents lists available at ScienceDirect

Applied Catalysis B: Environmental

journal homepage: www.elsevier.com/locate/apcatb

Cobalt phthalocyanine coordinated to pyridine-functionalized carbon nanotubes with enhanced CO_2 electroreduction

Minghui Zhu[a], Jiacheng Chen[a], Rong Guo[b], Jing Xu[a], Xiangchen Fang[b,**], Yi-Fan Han[a,c,*]

[a] State Key Laboratory of Chemical Engineering, East China University of Science and Technology, Shanghai 200237, China
[b] Dalian Research Institute of Petroleum and Petrochemicals, SINOPEC, 116045, China
[c] Research Center of Heterogeneous Catalysis and Engineering Sciences, School of Chemical Engineering and Energy, Zhengzhou University, Zhengzhou 450001, China

ARTICLE INFO

Keywords:
Carbon dioxide
Electroreduction
Carbon nanotube
Pyridine
Cobalt phthalocyanine

ABSTRACT

Electrochemical reduction of CO_2 is promising to utilize the intermittent renewable electricity and transform CO_2 into value-added products, simultaneously. Herein, we designed a cobalt phthalocyanine-based catalyst supported on pyridine-functionalized carbon nanotubes (CoPc-py-CNT). This novel hybrid catalyst exhibited a high activity (TOF_{CO}: 34.5 s^{-1} at −0.63 V *vs.* RHE) and selectivity (FE_{CO} > 98%) for electrochemical CO_2 reduction. To the best of our knowledge, it is the best one among all reported molecular based electrocatalysts for CO_2-to-CO conversion. Furthermore, structure characterizations (such as Raman and X-rays photoelectron spectroscopy), loading-dependent electrochemical analysis and mechanistic studies revealed that pyridine groups, through axial coordination with Co, not only functioned as physical promoters to improve the dispersion of cobalt phthalocyanine but also tuned the electronic structure of Co sites to increase the intrinsic turnover frequency.

1. Introduction

The environmental concern of the increasing CO_2 concentration in the atmosphere has inspired extensive research on new technologies that enable efficient and sustainable utilization of CO_2 [1]. Among the numerous solutions, electrochemical CO_2 reduction is an attractive technique which can harvest the intermittent renewable electricity and, in the meanwhile, produce value-added commodity chemicals [2–4]. Among the multitudinous catalysts that were developed [5–10], Co-based molecular complexes possess ultra-high selectivity toward CO, which is of industrial significance as it can be further transformed into a diversity of value-added products, including acids, esters, and alcohols *via* downstream catalytic processes [11–17].

Previous studies on molecular complexes for CO_2 reduction have revealed that reaction rates are improved by heterogenization, which leads to a high catalyst dispersion and therefore increases the number of available active sites [18–21]. The resulting high current densities particularly favor industrial application, which typically requires at least 100 mA/cm^2 [22]. Zhang et al. investigated the performance of cobalt phthalocyanine (CoPc) immobilized on different carbonaceous supports including carbon nanotubes (CNT), carbon black (CB) and reduced graphene oxide (RGO). A CoPc/CNT composite exhibited higher current density for electroreduction of CO_2 compared to those on other types of supports [23]. It has proved that CNT with a higher graphitic degree likely affords higher electron conductivity as well as better π–π interaction with CoPc. Besides, conductive polymers were also reported as feasible supports for heterogenization and could improve the overall catalytic performance [24].

An alternative strategy for improving the reactivity has implemented by tuning the electronic structure of the molecular complexes *via* functionalization. For instance, Abe et al. reported that turnover frequency (TOF) of CoPc could be improved by peripheral functionalization with eight butoxy (BuO) substituents [25]. This was attributed to the electron-donating nature of BuO that facilitated the coordination of CO_2 as well as the electron transfer from the catalyst to the adsorbed CO_2. An electron-withdrawing cyano substituted CoPc $(CN)_8$ catalyst was also reported to exhibit higher activity than plain CoPc molecules and was explained by the facilitation of Co activation as well as CO desorption [23,26]. In addition, perfluorinated cobalt phthalocyanine ($CoPcF_{16}$) has found to be more active than CoPc. The electron-withdrawing fluorine substituents were considered to protect the catalyst from poisoned by CO and make the active Co sites more accessible [27]. Functionalization of the macrocyclic ligand has also been extended to support modification, cobalt tetraphenylporphyrin

* Corresponding author at: State Key Laboratory of Chemical Engineering, East China University of Science and Technology, Shanghai 200237, China.
** Corresponding author.
E-mail addresses: fxc@ecust.edu.cn (X. Fang), yifanhan@ecust.edu.cn (Y.-F. Han).

https://doi.org/10.1016/j.apcatb.2019.03.047
Received 1 January 2019; Received in revised form 12 February 2019; Accepted 16 March 2019
Available online 18 March 2019

(CoTPP) attached to pyridine modified glassy carbon (GC) electrode was reported to achieve improved activity [27–29]. However, the planar substrate with a limited surface area and the resulted low catalytic performance limited the broader application as well as feasible mechanistic interpretation.

In our previous study, we showed that CoPc and its analogs tend to form inter-molecular stacking and agglomeration at high loadings [30]. Since TOFs were usually calculated based on the total number of molecular catalysts, they could be under-estimated if aggregation existed. This highlighted the importance of performing electrochemical studies at low catalyst loadings to unveil the intrinsic property of the catalysts. Unfortunately, previous studies were mainly performed at high loadings where aggregations were noticeable, reflected by the low TOFs and high Tafel slopes [30–33]. This hampered the rational design of cobalt-based molecular catalysts for CO_2 electroreduction.

In this work, we synthesized a new CoPc-based composite catalyst using pyridine-functionalized carbon nanotubes to anchor CoPc molecules and conducted a method of electronic tuning through direct axial ligation. More importantly, we elucidated the promotional mechanism of this axial coordination with loading-dependent electrochemical studies.

2. Experimental section

2.1. Catalyst preparation

Cobalt phthalocyanine (CoPc, β-form, Dye content 97%) was purchased from Sigma Aldrich and used as-purchased. Multiwall carbon nanotubes (purity: > 95%, OD: 10–20 nm) were purchased from US Research Nanomaterials, Inc. and further purified by soaking in a 6 M HCl solution overnight. Pyridine-functionalized carbon nanotubes (py-CNT) were synthesized following a reported method [34]. To prepare the CoPc-py-CNT composite, 20 mg of py-CNT and a certain amount of CoPc were dispersed in 4 ml *N*,*N*-dimethylformamide followed by 30 min sonication. The mixture was then vigorously stirred overnight in an oil-bath at 80 °C. Then, 50 μL of 5 wt.% Nafion solution (Sigma Aldrich) was added and the resulting mixture was further sonicated for 30 min to result in a well dispersed CoPc-py-CNT ink.

For characterizations, a certain amount of catalyst ink was drop casted on an aluminum foil and dried in the oven at 80 °C. The resulting powders were then collected for further analysis. To prepare working electrode, 15 μL of this catalyst ink was drop casted onto carbon paper disk (Toray, TGP-H-060) with a diameter of 12.7 mm and dried in the oven at 80 °C. Working electrodes containing CoPc-CNT or CoPc were prepared by the same method with different starting compositions for making the catalyst ink. Detailed ingredients and the corresponding CoPc loadings were presented in Table S1-3 in Supporting information (SI).

2.2. Material characterizations

The morphology of catalysts was analyzed using Transmission Electron Microscopy (TEM, FEI Tecnai G2 F20 S-Twin) with an accelerating voltage of 200 kV. The samples were prepared by directly suspending the catalyst in ultrapure water with ultrasonic treatment. Then 2–3 drops of this slurry were deposited on a copper microscope grid covered with perforated carbon (Beijing Zhongjingkeyi Technology) and dried with an infrared lamp.

Raman spectrum were collected using a confocal Raman spectroscopy (LabRAM HR, Horiba) equipped with a visible 514.5 nm Ar^+ laser and a high-grade Leica microscope (long working distance objective 50×). Single crystal silicon was used for position correction. The confocal pore size was set to 300 μm for all tests.

X-ray photoelectron spectroscopy (XPS) analysis was obtained using a Thermo ESCALAB 250Xi spectrometer equipped with a monochromatic AlK radiation source (1486.6 eV, pass energy 20.0 eV). The background pressure in the analysis chamber was kept below 3.0×10^{-7} mbar during data acquisition. High-resolution scans were made with a dwell time of 0.1 s and a step size of 0.05 eV. The binding energies (BEs) were calibrated using the C1s peak at 284.8 eV as a reference.

2.3. Electrochemical measurements

The electrochemical performance for CO_2 reduction was tested in a customized H-type cell separated by a Nafion-117 membrane [30]. A platinum foil was used as a counter electrode and a leak-free Ag/AgCl electrode (LF-2, Innovative Instrument Inc.) was used as the reference electrode. Prior to experiments, 1.75 mL of electrolyte was added into the working and counter compartment, respectively. Cells were purged with CO_2 for 10 min prior to electrochemical tests. A CHI650E potentiostat was employed to record the electrochemical responses. The resistance between the reference electrode and working electrode was measured using a Potential Electrochemical Impedance Spectroscopy (PEIS) and manually compensated. During electrolysis, gas products were analyzed by an on-line gas chromatograph (Ruimin GC 2060, Shanghai) equipped with a Hayesep-D column, a thermal conductivity detector (TCD) and a flame ionization detector (FID).

The electrolyte for cyclic voltammetry measurement, steady-state activity measurement, CO_2 order-dependence tests and Tafel slope tests was operated in a 0.2 M sodium bicarbonate (Sigma Aldrich) solution. To test the order-dependence on bicarbonate at constant ionic strength, sodium perchlorate (Sigma Aldrich) was used as a supporting electrolyte [35]. In these experiments, for a desired sodium bicarbonate concentration, the total sodium ion concentration was kept at 0.5 M by adjusting the sodium perchlorate amount. We choose a higher concentration here to ensure an evaluation at a wider range of bicarbonate concentrations. For CO_2 order-dependence tests, the total flow rate and pressure were kept constant by adding in a diluent stream of N_2.

3. Results and discussion

3.1. Catalyst synthesis and characterizations

CoPc-py-CNT composites were prepared from covalent functionalization of CNT (py-CNT). In this approach, pyridine groups (py) were firstly anchored on the walls of CNTs, taking advantage of the diazonium reaction. A controlled amount of CoPc was then coordinated to py-CNT through the bond formation between the nitrogen atom in pyridine and Co center in CoPc (Fig. 1a). By TEM images, we found that the as-prepared hybrid catalyst possessed a clean surface morphology without observable aggregations (Fig. 1b), it indicated that CoPc was well distributed along the carbon nanotubes.

Fig. 1c displays the Raman spectrum of pristine CNT and pyridine functionalized CNT. Two peaks at 1350 and 1580 cm^{-1} can be assigned to the D band and the G band, originating from the disorder-induced C—C vibration and the tangential E_{2g} sp^2 bonded C=C stretching vibration, respectively [36]. We then calculated the integrated intensity ratio of the D to the G peak (I_D/I_G), which is considered as an indicator for the degree of disorder. Pyridine functionalized carbon nanotube (py-CNT) exhibited slightly higher I_D/I_G ratio (I_D/I_G = 1.1) than pristine CNT (I_D/I_G = 0.9), and thus probably exposed a larger number of defects as a result of pyridine functionalization [37].

The XPS Co 2p spectrum reveals Co $2p_{3/2}$ peak at 781.3 eV and $2p_{1/2}$ peak at 796.5 eV (Fig. 1d) for unsupported CoPc. The positions of both peaks remained unperturbed for CoPc-CNT, reflecting the negligible electronic interaction between CNT and Co atoms in CoPc. On the other hand, the Co 2p core level spectra in the CoPc-py-CNT composite became broader and slightly shifted to 780.7 eV and 795.8 eV, respectively. As Co ions can coordinate with pyridine groups of CoPc-Py-CNT at the axial direction, the extra ligand led to an increase in electron density around Co, resulting in a less positive valent state than CoPc-

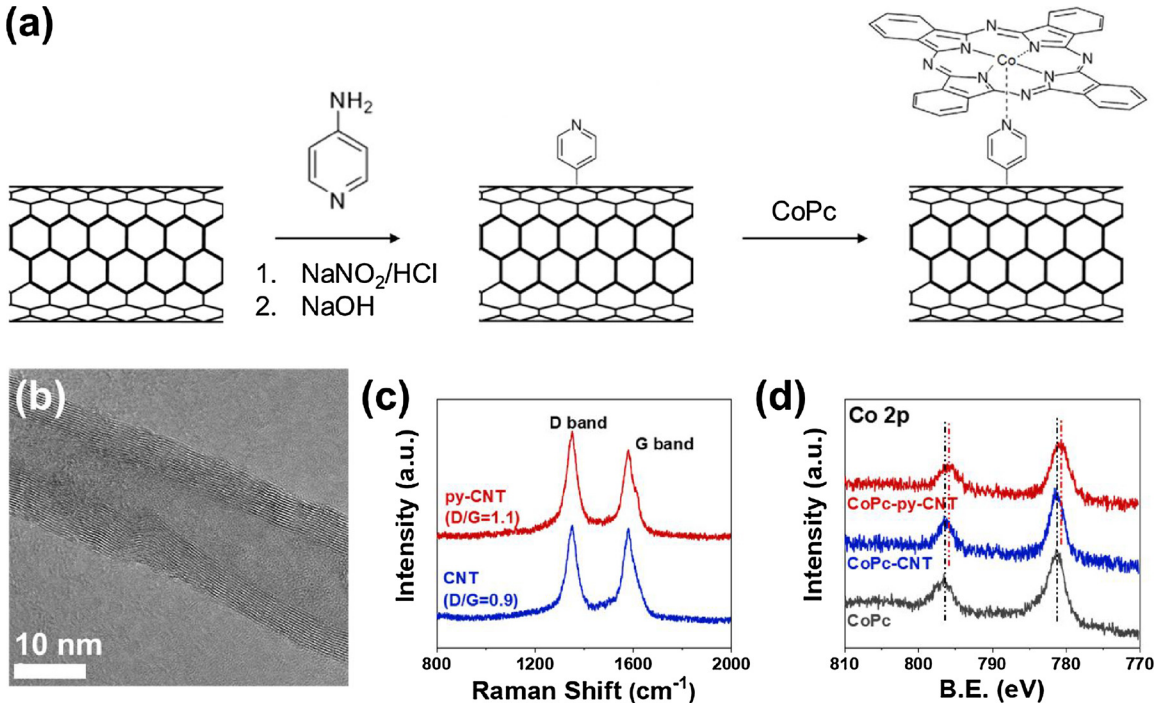

Fig. 1. (a) Synthesis of CoPc-py-CNT composite. (b) a typical TEM image of CoPc-py-CNT (loading amount: 5×10^{-9} mol/cm^2) showing smooth surface free of any observable aggregations. (c) Raman spectrum of py-CNT and pristine CNT and (d) Co 2p spectra of free-standing CoPc, CoPc-CNT and CoPc-py-CNT.

CNT [37]. As a result, the peak positions of Co 2p were shifted down. The broader peaks may suggest that not all CoPc molecules are coordinated to pyridine groups.

3.2. Potential-dependent electrochemical analysis

To investigate the electrocatalytic activity of the CoPc-Py-CNT composite for CO_2 reduction, the as-synthesized composite catalysts were tested in a customized low volume cell. Cyclic voltammetry was first performed in the electrolyte pre-saturated with CO_2, which showed prominent reductive current at potentials more negative than -0.4 V *vs.* RHE (Fig. 2a). Among three catalysts, CoPc-py-CNT exhibited the highest current densities, followed by CoPc-CNT. The unsupported CoPc had the least activity due to its lowest dispersion. During the steady-state electrolysis, current densities were all stable (Fig. 2b) with a maximum reductive current of ~9.9 mA/cm^2 achieved on CoPc-py-CNT at −0.73 V *vs.* RHE. We detected that H_2 and CO were the major products (Fig. 2c, Table S4-5) with a gas chromatography (GC). The product distribution has found to be dependent on the applied potential. At a low potential of −0.53 V *vs.* RHE, the Faradaic efficiency for CO (FE_{CO}) was determined to be 82% for the CoPc-CNT composite. The FE_{CO} increased with larger overpotential applied and reached over 95% at potentials more negative than −0.6 V *vs.* RHE. While exhibiting similar FE_{CO} at high overpotentials, the CoPc-py-CNT composite was more selective toward CO at less reductive polarizations and still maintained a high FE_{CO} of 91% at −0.53 V *vs.* RHE. For pure CNT, the reduction current density at −0.73 V *vs.* RHE was only 0.1 mA/cm^2, and only H_2 could be detected as the reduction product (Table S7). Fig. 2d displays the partial current densities of the reduction products over CoPc-CNT and CoPc-py-CNT at various potentials. The production rate of CO over CoPc-py-CNT was higher than that for the CoPc-CNT catalyst. These results indicate that CoPc-py-CNT not only has higher catalytic activity but also enhanced product selectivity.

3.3. Loading-dependent electrochemical analysis

As previously described, metal phthalocyanine molecules tend to form inter-molecular stacking and aggregation [38–41]. It was then essential to deconvolute the contributing factors of the improved electrocatalytic performance of CoPc-py-CNT. Therefore, we performed loading-dependent electrochemical analysis by evaluating a wide range of CoPc loadings (from 1×10^{-11} to 1×10^{-7} mol/cm^2) and calculated the TOFs which is defined as the number of CO molecules produced per active site per unit time.

The total number of active sites could be estimated by integrating the cyclic voltammogram peak for the $Co^{II} \rightarrow Co^{I}$ transition during a standard cyclic voltammetry process [24,31,42]. The accuracy of such approach was, however, limited especially at ultra-low catalyst loadings used in this study. Furthermore, the integrated redox signal corresponds to all Co sites that are electron-accessible, hence overestimates the number of Co sites active for electroreduction of CO_2 which requires simultaneous availability to CO_2, proton, and electron. Alternatively, TOF could also be calculated based on the total number of CoPc deposited on the carbon paper. Due to the existence of catalyst aggregation and transport limitation, calculated TOF only represent lower bound of the intrinsic activity for CoPc. Nevertheless, near-intrinsic TOF could be approached at reduced CoPc loadings where molecular stacking and transport limitation were minimized.

Catalysts with different CoPc loadings exhibited similar onset potentials (−0.4 V *vs.* RHE) according to the cyclic voltammetry analysis (Fig. S1). At a constant potential of −0.63 V *vs.* RHE, TOF_{CO} of unsupported CoPc gradually increased with decreasing the catalyst loading amount and approached 20 s^{-1} at loadings below 2×10^{-11} mol/cm^2, which can be considered as a near-intrinsic TOF_{CO} for CoPc (Fig. 3). The CoPc-CNT composite initially showed a comparable TOF_{CO} of 0.19 s^{-1} at the highest loading, which took off more rapidly than CoPc at lower loadings. The TOFs then started to level off at a loading of 1×10^{-10} mol/cm^2, and eventually, were almost equal to CoPc. The comparable TOFs (~18 s^{-1}) at the lowest loadings, which represent the near-intrinsic activity of CoPc, demonstrated that addition of CNT did not affect the intrinsic activity. And, the increase in TOF_{CO} in the loading region of 2×10^{-8} mol/cm^2–1×10^{-10} mol/cm^2 is exclusively a consequence of higher catalyst dispersion. In contrast, while CoPc-py-CNT had a similar TOF-loading trend compared to CoPc-CNT, it

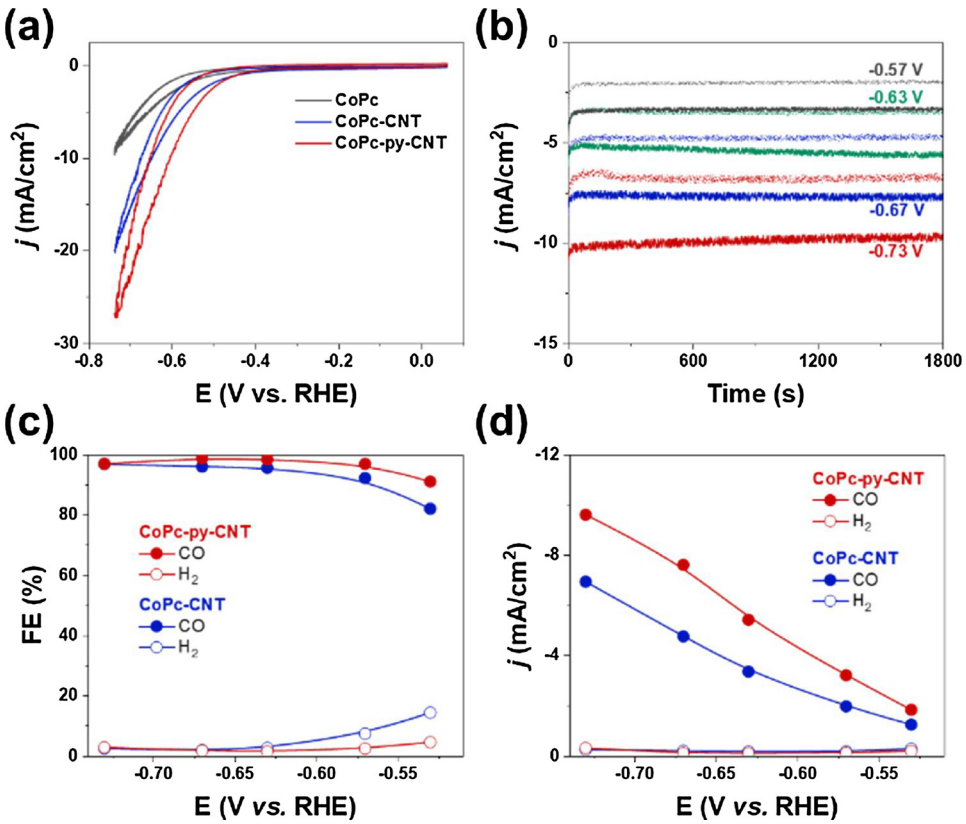

Fig. 2. (a) Cyclic voltammograms recorded at a sweep rate of 10 mV/s on CoPc, CoPc-CNT, and CoPc-py-CNT. (b) Current densities of CoPc-py-CNT (solid line) and CoPc-CNT (dotted line) at various potentials. (c) Faradaic efficiencies and (d) partial current densities of CO_2 reduction products for CoPc-CNT in comparison with CoPc-py-CNT at various potentials. CoPc loading is 5×10^{-9} mol/cm^2.

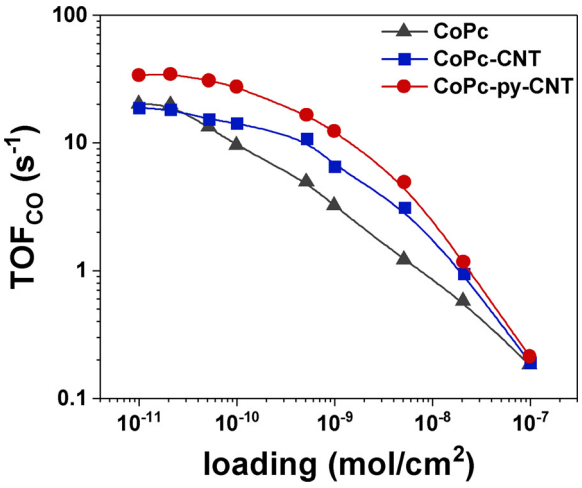

Fig. 3. TOF_{CO} comparison of CoPc, CoPc-CNT, and CoPc-py-CNT at various CoPc loadings.

exhibited consistently higher TOF_{CO} even at the lowest catalyst loading, reaching the maximum value of 34.5 s^{-1}. To the best of our knowledge, this is among the highest TOFs that have ever been reported for CO_2 electroreduction to CO on the molecular complex in aqueous media (Table S8). We tested the long-term stability of CoPc-py-CNT at a CoPc loading of 5×10^{-11} mol/cm^2, both the current density and faradaic efficiencies stayed relatively stable at a polarization of −0.63 V *vs.* RHE for up to 12 h (Fig. S2). During the stability test, a total amount of ca.72 umol CO was produced, corresponding to an outstanding turnover number (TON) of 1.4 million. The increased near-intrinsic TOF_{CO} by CoPc-py-CNT also clearly demonstrates the electronic effect by pyridine coordination.

3.4. Reaction mechanism

Given the distinct trends of TOF_{CO}, we sought to mechanistically understand the promotional mechanism of pyridine coordination. It was well known that Co^I sites are responsible for electroreduction of CO_2, however, the rate-determining-step (RDS) has received less attention [43,44]. Mechanistic studies in the literature were usually performed at high catalyst loadings with the existence of molecular aggregation and transport limitations. This was reflected by the reported high Tafel slopes, which ranged from 165 to 550 mV/dec. [27,31,32,45] As a result, transport limitations coexisted with kinetic limitations and complicated the mechanistic interpretations.

Furthermore, we performed Tafel analysis on the CoPc composite at two different loadings. At a high loading of 5×10^{-9} mol/cm^2, a Tafel slope for CoPc-CNT was 206 mV/dec, which clearly indicated the existence of transport limitation (Fig. 4a) [31]. In contrast, CoPc-py-CNT exhibited a much lower Tafel slope at the same loading (143 mV/dec); the transport limitation still existed, demonstrating indirectly that the dispersion of CoPc can be improved by axial pyridine coordination. On the other hand, both CoPc-CNT and CoPc-py-CNT presented similar Tafel slopes at around 118 mV/dec when CoPc loading was decreased by two orders of magnitude to 5×10^{-11} mol/cm^2 (Fig. 4b). It indicates that the reaction became kinetically limited and is consistent with a rate-limiting one electron transfer step [35].

Next, we conducted order-dependence measurements at the loading of 5×10^{-11} mol/cm^2 and at polarization of −0.63 V *vs.* RHE, which falls in the linear Tafel region in order to minimize transport limitations. The order-dependence of the partial current density for CO (j_{CO}) on CO_2 partial pressure revealed a first-order dependence for CoPc-CNT (0.93) and CoPc-py-CNT (1.05), indicating that CO_2 participates in the rate-determining step (Fig. 4c). Both catalysts exhibited a zeroth-order with respect to bicarbonate (Fig. 4d). The pH value of each electrolyte solution during the bicarbonate order dependent analysis was measured, and the values were closely related to the concentration of bicarbonate (Table S9). Similarly, plots of log(j_{CO}) against pH values

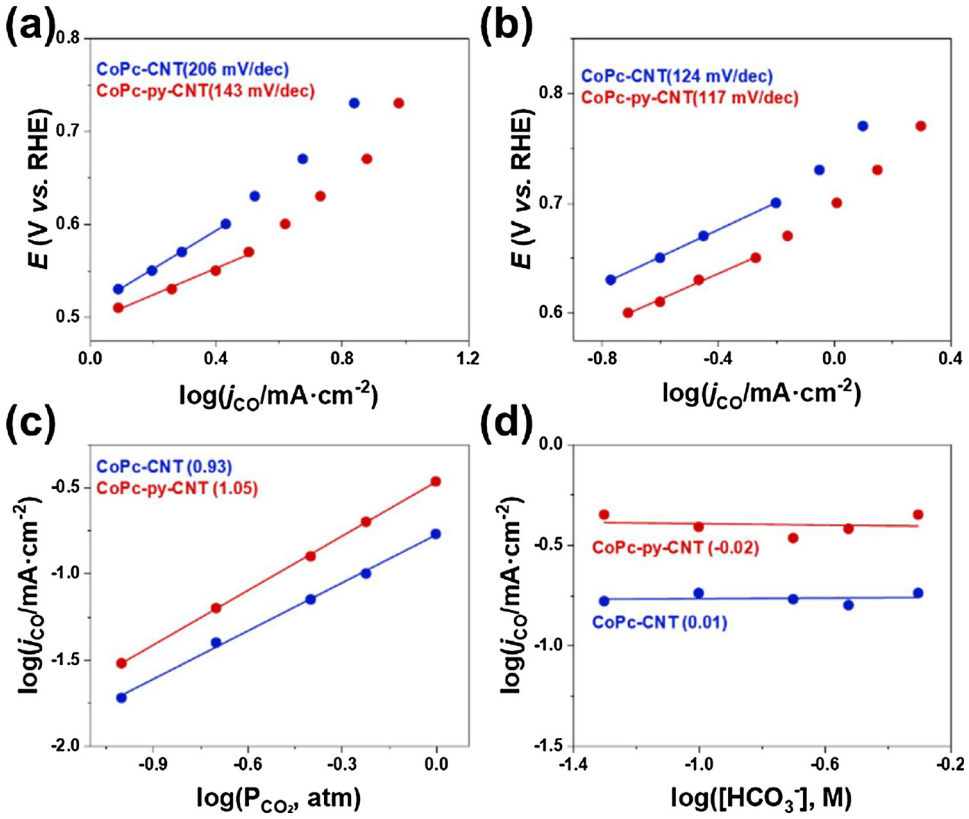

Fig. 4. Tafel plots for CoPc-CNT and CoPc-py-CNT at CoPc loading of (a) 5×10^{-9} mol/cm^2 and (b) 5×10^{-11} mol/cm^2, (c) CO partial current density (j_{CO}) on CoPc-CNT and CoPc-py-CNT as a function of (c) CO_2 partial pressure and (d) bicarbonate concentration. CoPc loading: 5×10^{-11} mol/cm^2.

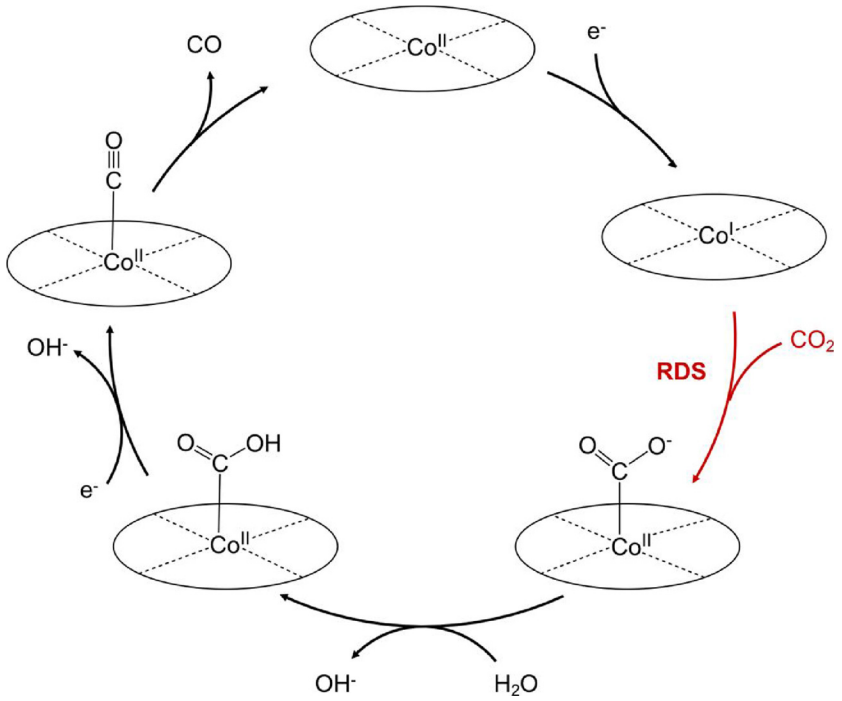

Scheme 1. Proposed Mechanism for CO_2 electroreduction to CO over a catalyst of immobilized CoPc on CNT.

revealed a zeroth-order on pH value for CoPc-CNT and CoPc-py-CNT (Fig. S3). Those results suggested that bicarbonate and proton do not participate in the rate-determining step of CO_2 electroreduction. By integrating the Tafel slopes, CO_2 order-dependence and bicarbonate order-dependence, we concluded that both CoPc-CNT and CoPc-py-CNT have exactly the same rate-determining step, which is the binding of CO_2 and the simultaneous electron-transfer process (Scheme 1). This assertion is also consistent with previous mechanistic study on free-standing CoPc [30].

3.5. Promotional mechanism of pyridine coordination

By integrating the structure characterization results (Raman and XPS spectroscopy), loading-dependent electrochemical analysis and mechanistic studies, the promotional mechanism of pyridine coordination can be rationalized. The pyridine functionalities could form a Co-N coordination bond with CoPc, which is much stronger than the van der Waals π–π interaction between CoPc molecules. This stronger interaction could function as a driving force to spread CoPc molecules more evenly alongside the carbon nanotube surface.

On the other hand, axial pyridine coordination with a transition metal site has been widely utilized in the field of inorganic chemistry and reported to tune the electronic structure of the attached metal ions [46–48]. The axial coordination between CoPc and pyridine functionalized CNT led to a higher charge density in the CoPc-py-CNT system and raised the energy of the Co d_{z2} orbital; it is consistent with XPS results, showing a decreased Co 2p binding energy for CoPc-py-CNT. The electron-rich Co sites became more nucleophilic and could bind the Lewis acidic CO_2 molecules more strongly. Since the binding of CO_2 involves in the rate-determining step of CO_2 electroreduction, a facilitated CO_2 binding process would result in a promoted CO_2 reduction reaction.

4. Conclusions

To summarize, we report a CoPc based catalyst that is supported on pyridine-functionalized carbon nanotubes. This hybrid catalyst exhibited a high activity (TOF_{CO}: 34.5 s^{-1} at −0.63 V *vs.* RHE) and selectivity (FE_{CO} > 98%) for electrochemical CO_2 reduction. To the best of our knowledge, it is the best one among all reported molecular based electrocatalysts for CO_2-to-CO conversion. We found that the pyridine groups actively coordinate with Co atoms and increase the surrounding electron densities, thus, not only improve the dispersion of CoPc at high loadings but increase the intrinsic activity of CoPc molecules. The mechanistic studies elucidated that the rate-determining step of CO_2 electroreduction on CoPc is the binding of CO_2 and the simultaneous electron transfer, which are not perturbed by the axial pyridine coordination. Our work also demonstrates a strategy to decouple the physical effect and electronic effect, which is essential for the evaluation and rational design of molecular electrocatalysts.

Acknowledgments

We gratefully thank the Start-up Grant of East China University of Science and Technology (SG1503A003), National Key R&D Program of China (2018YFB0605803) and Fundamental Research Funds for the Central Universities (222201718002).

Appendix A. Supplementary data

Supplementary material related to this article can be found, in the online version, at doi:https://doi.org/10.1016/j.apcatb.2019.03.047.

References

[1] S. Manabe, R.J. Stouffer, Sensitivity of a global climate model to an increase of CO_2 concentration in the atmosphere, J. Geophys. Res. 85 (1980) 5529, https://doi.org/10.1029/JC085iC10p05529.
[2] S. Chu, A. Majumdar, Opportunities and challenges for a sustainable energy future, Nature 488 (2012) 294–303, https://doi.org/10.1038/nature11475.
[3] N.S. Lewis, D.G. Nocera, Powering the planet: chemical challenges in solar energy utilization, Proc. Natl. Acad. Sci. U. S. A. 103 (2006) 15729–15735, https://doi.org/10.1073/pnas.0603395103.
[4] Z.J. Schiffer, K. Manthiram, Electrification and decarbonization of the chemical industry, Joule 1 (2017) 10–14, https://doi.org/10.1016/j.joule.2017.07.008.
[5] Z.W. Seh, J. Kibsgaard, C.F. Dickens, I. Chorkendorff, J.K. Nørskov, T.F. Jaramillo, Combining theory and experiment in electrocatalysis: insights into materials design, Science 355 (2017) 4998–5009, https://doi.org/10.1126/science.aad4998.
[6] B. Khezri, A.C. Fisher, M. Pumera, CO_2 reduction: the quest for electrocatalytic materials, J. Mater. Chem. A 5 (2017) 8230–8246, https://doi.org/10.1039/C6TA09875D.
[7] T. Zheng, K. Jiang, H. Wang, Recent advances in electrochemical CO_2-to-CO conversion on heterogeneous catalysts, Adv. Mater. 30 (2018) 1802066, https://doi.org/10.1002/adma.201802066.
[8] L. Lu, X. Sun, J. Ma, D. Yang, H. Wu, B. Zhang, J. Zhang, B. Han, Highly efficient electroreduction of CO_2 to methanol on palladium-copper bimetallic aerogels, Angew. Chem. Int. Ed. 57 (2018) 14149–14153, https://doi.org/10.1002/anie.201808964.
[9] D. Bohra, I. Ledezma-Yanez, G. Li, W. de Jong, E.A. Pidko, W.A. Smith, Lateral adsorbate interactions inhibit HCOO-while promoting CO selectivity for CO_2 electrocatalysis on silver, Angew. Chem. Int. Ed. (2018) 1–5, https://doi.org/10.1002/anie.201811667.
[10] X. Wang, Z. Chen, X. Zhao, T. Yao, W. Chen, R. You, C. Zhao, G. Wu, J. Wang, W. Huang, J. Yang, X. Hong, S. Wei, Y. Wu, Y. Li, Regulation of coordination number over single Co sites: triggering the efficient electroreduction of CO_2, Angew. Chem. Int. Ed. 57 (2018) 1944–1948, https://doi.org/10.1002/anie.201712451.
[11] S. Sato, K. Saita, K. Sekizawa, S. Maeda, T. Morikawa, Low-energy electrocatalytic CO2 reduction in water over Mn-complex catalyst electrode aided by a nanocarbon support and K+ cations, ACS Catal. 8 (2018) 4452–4458, https://doi.org/10.1021/acscatal.8b01068.
[12] C. Costentin, M. Robert, J.-M. Savéant, Current issues in molecular catalysis illustrated by iron porphyrins as catalysts of the CO_2-to-CO electrochemical conversion, Acc. Chem. Res. 48 (2015) 2996–3006, https://doi.org/10.1021/acs.accounts.5b00262.
[13] E.E. Benson, C.P. Kubiak, A.J. Sathrum, J.M. Smieja, Electrocatalytic and homogeneous approaches to conversion of CO_2 to liquid fuels, Chem. Soc. Rev. 38 (2009) 89–99, https://doi.org/10.1039/B804323J.
[14] Z. Zhang, J. Zhang, X. Wang, R. Si, J. Xu, Y.-F. Han, Promotional effects of multi-walled carbon nanotubes on iron catalysts for Fischer-Tropsch to olefins, J. Catal. 365 (2018) 71–85, https://doi.org/10.1016/j.jcat.2018.05.021.
[15] T. Chen, J. Su, Z. Zhang, C. Cao, X. Wang, R. Si, X. Liu, B. Shi, J. Xu, Y.-F. Han, Structure evolution of Co–CoO_x interface for higher alcohol synthesis from syngas over Co/CeO_2 catalysts, ACS Catal. 8 (2018) 8606–8617, https://doi.org/10.1021/acscatal.8b00453.
[16] Y. Zhang, D. Fu, X. Liu, Z. Zhang, C. Zhang, B. Shi, J. Xu, Y.-F. Han, Operando spectroscopic study of dynamic structure of Iron oxide catalysts during CO_2 hydrogenation, ChemCatChem 10 (2018) 1272–1276, https://doi.org/10.1002/cctc.201701779.
[17] G. Yin, X. Huang, T. Chen, W. Zhao, Q. Bi, J. Xu, Y. Han, F. Huang, Hydrogenated blue titania for efficient solar to chemical conversions: preparation, characterization, and reaction mechanism of CO_2 reduction, ACS Catal. 8 (2018) 1009–1017, https://doi.org/10.1021/acscatal.7b03473.
[18] C.M. Lieber, N.S. Lewis, Catalytic reduction of carbon dioxide at carbon electrodes modified with cobalt phthalocyanine, J. Am. Chem. Soc. 106 (1984) 5033–5034, https://doi.org/10.1021/ja00329a082.
[19] C. Sun, R. Gobetto, C. Nervi, Recent advances in catalytic CO_2 reduction by organometal complexes anchored on modified electrodes, New J. Chem. 40 (2016) 5656–5661, https://doi.org/10.1039/C5NJ03426D.
[20] N. Furuya, K. Matsui, Electroreduction of carbon dioxide on gas-diffusion electrodes modified by metal phthalocyanines, J. Electroanal. Chem. 271 (1989) 181–191, https://doi.org/10.1016/0022-0728(89)80074-9.
[21] M. Zhu, J. Chen, L. Huang, R. Ye, J. Xu, Y.-F. Han, Covalently grafted cobalt porphyrin on carbon nanotube for efficient CO_2 electroreduction, Angew. Chem. Int. Ed. (2019), https://doi.org/10.1002/ange.201900499.
[22] C. Dinh, T. Burdyny, M.G. Kibria, A. Seifitokaldani, C.M. Gabardo, F.P. García de Arquer, A. Kiani, J.P. Edwards, P. De Luna, O.S. Bushuyev, C. Zou, R. Quintero-Bermudez, Y. Pang, D. Sinton, E.H. Sargent, CO_2 electroreduction to ethylene via hydroxide-mediated copper catalysis at an abrupt interface, Science 360 (2018) 783–787, https://doi.org/10.1126/science.aas9100.
[23] X. Zhang, Z. Wu, X. Zhang, L. Li, Y. Li, H. Xu, X. Li, X. Yu, Z. Zhang, Y. Liang, H. Wang, Highly selective and active CO_2 reduction electrocatalysts based on cobalt phthalocyanine/carbon nanotube hybrid structures, Nat. Commun. 8 (2017) 14675–14682, https://doi.org/10.1038/ncomms14675.
[24] W.W. Kramer, C.C.L. McCrory, Polymer coordination promotes selective CO_2 reduction by cobalt phthalocyanine, Chem. Sci. 7 (2016) 2506–2515, https://doi.org/10.1039/C5SC04015A.
[25] T. Abe, F. Taguchi, T. Yoshida, S. Tokita, G. Schnurpfeil, D. Wöhrle, M. Kaneko, Electrocatalytic CO_2 reduction by cobalt octabutoxyphthalocyanine coated on graphite electrode, J. Mol. Catal. A: Chem. 112 (1996) 55–61, https://doi.org/10.1016/1381-1169(96)00242-7.
[26] T. Abe, H. Imaya, T. Yoshida, S. Tokita, D. Schlettwein, D. Wohrle, M. Kaneko, Electrochemical CO_2 reduction catalyzed by cobalt octacyanophthalocyanine and its mechanism, J. Porphyr. Phthalocyanines 1 (1997) 315–321, https://doi.org/10.1002/(sici)1099-1409(199710)1:4<315::aid-jpp35>3.0.co;2-v.
[27] N. Morlanés, K. Takanabe, V. Rodionov, Simultaneous reduction of CO_2 and splitting of H_2O by a single immobilized cobalt phthalocyanine electrocatalyst, ACS Catal. 6 (2016) 3092–3095, https://doi.org/10.1021/acscatal.6b00543.
[28] T. Atoguchi, A. Aramata, A. Kazusaka, M. Enyo, Cobalt–tetraphenylporphyrin–pyridine complex fixed on a glassy carbon electrode and its prominent catalytic activity for reduction of carbon dioxide, J. Chem. Soc. Chem. Commun. 0 (1991) 156–157, https://doi.org/10.1039/C39910000156.
[29] T. Atoguchi, A. Aramata, A. Kazusaka, M. Enyo, Electrocatalytic activity of CoII TPP-pyridine complex modified carbon electrode for CO_2 reduction, J. Electroanal. Chem. Interfacial Electrochem. 318 (1991) 309–320, https://doi.org/10.1016/

0022-0728(91)85312-D.
[30] M. Zhu, R. Ye, K. Jin, N. Lazouski, K. Manthiram, Elucidating the reactivity and mechanism of CO_2 electroreduction at highly dispersed cobalt phthalocyanine, ACS Energy Lett. 3 (2018) 1381–1386, https://doi.org/10.1021/acsenergylett.8b00519.
[31] S. Lin, C.S. Diercks, Y.-B. Zhang, N. Kornienko, E.M. Nichols, Y. Zhao, A.R. Paris, D. Kim, P. Yang, O.M. Yaghi, C.J. Chang, Covalent organic frameworks comprising cobalt porphyrins for catalytic CO_2 reduction in water, Science 349 (2015) 1208–1213, https://doi.org/10.1126/science.aac8343.
[32] N. Kornienko, Y. Zhao, C.S. Kley, C. Zhu, D. Kim, S. Lin, C.J. Chang, O.M. Yaghi, P. Yang, Metal–organic frameworks for electrocatalytic reduction of carbon dioxide, J. Am. Chem. Soc. 137 (2015) 14129–14135, https://doi.org/10.1021/jacs.5b08212.
[33] H.H. Wu, M. Zeng, X. Zhu, C.C. Tian, B.B. Mei, Y. Song, X.L. Du, Z. Jiang, L. He, C.G. Xia, S. Dai, Defect engineering in polymeric cobalt phthalocyanine networks for enhanced electrochemical CO_2 reduction, ChemElectroChem 5 (2018) 2717–2721, https://doi.org/10.1002/celc.201800806.
[34] M.K. Bayazit, L.S. Clarke, K.S. Coleman, N. Clarke, Pyridine-functionalized single-walled carbon nanotubes as gelators for poly(acrylic acid) hydrogels, J. Am. Chem. Soc. 132 (2010) 15814–15819, https://doi.org/10.1021/ja1076662.
[35] A. Wuttig, Y. Yoon, J. Ryu, Y. Surendranath, bicarbonate is not a general acid in Au-catalyzed CO_2 electroreduction, J. Am. Chem. Soc. 139 (2017) 17109–17113, https://doi.org/10.1021/jacs.7b08345.
[36] M.S. Dresselhaus, G. Dresselhaus, R. Saito, A. Jorio, Raman spectroscopy of carbon nanotubes, Phys. Rep. 409 (2005) 47–99, https://doi.org/10.1016/j.physrep.2004.10.006.
[37] M.S. Dresselhaus, A. Jorio, M. Hofmann, G. Dresselhaus, R. Saito, Perspectives on carbon nanotubes and graphene Raman spectroscopy, Nano Lett. 10 (2010) 751–758, https://doi.org/10.1021/nl904286r.
[38] J. Mizuguchi, π–π interactions of magnesium phthalocyanine as evaluated by energy partition analysis, J. Phys. Chem. A 105 (2001) 10719–10722, https://doi.org/10.1021/jp011169h.
[39] P. Erk, H. Hengelsberg, M.F. Haddow, R. van Gelder, The innovative momentum of crystal engineering, CrystEngComm 6 (2004) 474, https://doi.org/10.1039/b409282a.
[40] H.A. Moynihan, G. Claudon, Direction of copper phthalocyanine crystallization using in situ generated tethered phthalocyanines, CrystEngComm 12 (2010) 2695, https://doi.org/10.1039/c004048g.
[41] B. Dhara, K. Tarafder, P.K. Jha, S.N. Panja, S. Nair, P.M. Oppeneer, N. Ballav, Possible room-temperature ferromagnetism in self-assembled ensembles of Paramagnetic and diamagnetic molecular semiconductors, J. Phys. Chem. Lett. 7 (2016) 4988–4995, https://doi.org/10.1021/acs.jpclett.6b02063.
[42] N. Han, Y. Wang, L. Ma, J. Wen, J. Li, H. Zheng, K. Nie, X. Wang, F. Zhao, Y. Li, J. Fan, J. Zhong, T. Wu, D.J. Miller, J. Lu, S.-T. Lee, Y. Li, Supported cobalt polyphthalocyanine for high-performance electrocatalytic CO_2 reduction, Chem 3 (2017) 652–664, https://doi.org/10.1016/j.chempr.2017.08.002.
[43] C.L. Yao, J.C. Li, W. Gao, Q. Jiang, Cobalt-porphine catalyzed CO_2 electro-reduction: a novel protonation mechanism, Phys. Chem. Chem. Phys. 19 (2017) 15067–15072, https://doi.org/10.1039/C7CP01881A.
[44] J. Shen, M.J. Kolb, A.J. Göttle, M.T.M. Koper, DFT study on the mechanism of the electrochemical reduction of CO_2 catalyzed by cobalt porphyrins, J. Phys. Chem. C 120 (2016) 15714–15721, https://doi.org/10.1021/acs.jpcc.5b10763.
[45] X.-M. Hu, M.H. Rønne, S.U. Pedersen, T. Skrydstrup, K. Daasbjerg, Enhanced catalytic activity of cobalt porphyrin in CO_2 electroreduction upon immobilization on carbon materials, Angew. Chem. Int. Ed. 56 (2017) 6468–6472, https://doi.org/10.1002/anie.201701104.
[46] M. Brewer, D. Khasnis, M. Buretea, M. Berardini, T.J. Emge, J.G. Brennan, Pyridine coordination complexes of the divalent ytterbium chalcogenolates $Yb(EPh)_2$ (E = S, Se, Te), Inorg. Chem. 33 (1994) 2743–2747, https://doi.org/10.1021/ic00091a013.
[47] R. Patra, S. Bhowmik, S.K. Ghosh, S.P. Rath, Effects of axial pyridine coordination on a saddle-distorted porphyrin macrocycle: stabilization of hexa-coordinated high-spin Fe(iii) and air-stable low-spin iron(ii) porphyrinates, Dalton Trans. 39 (2010) 5795, https://doi.org/10.1039/b924742d.
[48] J.B. Cornelius, J. McCracken, R.B. Clarkson, R.L. Belford, J. Peisach, Electron spin echo envelope modulation angle selection studies of axial pyridine coordination to copper(II) benzoylacetonate, J. Phys. Chem. 94 (1990) 6977–6982, https://doi.org/10.1021/j100381a013.